# Orbital alignment cross sections by stimulated emission probing : the state-to-state Ca Rydberg process Ca(4s17d^1D_2)+Xe->Ca(4s18p^1P_1)+Xe

# Orbital alignment cross sections by stimulated emission probing: The state-to-state Ca Rydberg process $Ca(4s17d\ ^1D_2)+Xe \rightarrow Ca(4s18p\ ^1P_1)+Xe$

Eileen M. Spain,[a] Mark J. Dalberth, Paul D. Kleiber,[b] and Stephen R. Leone[c]
*Joint Institute for Laboratory Astrophysics, National Institute of Standards and Technology, University of Colorado, Boulder, Colorado 80309 and the Department of Chemistry and Biochemistry, University of Colorado, Boulder, Colorado 80309*

Stefan S. Op de Beek and Jan P. J. Driessen
*Physics Department, Eindhoven University of Technology, P.O. Box 513, 5600 MB Eindhoven, The Netherlands*

(Received 10 January 1995; accepted 22 March 1995)

The initial state alignment effect vs relative velocity is measured for a state-to-state Ca Rydberg collisional energy transfer process. The stimulated emission detection method is used to determine the alignment effect for the $n,l$-changing transition: $Ca(4s17d\ ^1D_2)+Xe \rightarrow Ca(4s18p\ ^1P_1)+Xe+\Delta E=-1.7\ cm^{-1}$. The rate of electronic energy transfer in this state-changing collision is observed to vary with the direction of the Rydberg electron charge cloud relative to the collision axis. Both the expected $\cos(4\beta)$ and $\cos(2\beta)$ dependencies are observed. The alignment data are analyzed to obtain the relative cross sections for the individual $Ca(^1D_2)$ magnetic sublevels. The values of the $m$-sublevel cross sections $\sigma^0:\sigma^{|1|}:\sigma^{|2|}$ are $1.13\pm0.02:1.11\pm0.02:0.83\pm0.02$. Qualitative interpretations of the relative cross sections in terms of both molecular (van der Waals) Born–Oppenheimer potentials and the impulse approximation are presented. 

## I. INTRODUCTION

The large size of a Rydberg atom suggests that it would undergo unique collision dynamics since the outer electron and cation core may be considered as separate scatterers, as first recognized by Fermi.[1] Depending on the Rydberg atom-collision partner interaction, the level of excitation in the Rydberg atom, and the nature of the collisional process, the relative contributions of the electron-perturber and ionic core-perturber interactions may vary. This is because tuning the principal quantum number, $n$, of the Rydberg state can alter important dynamical parameters such as the electron orbital velocity, period of electron orbit compared to collision time with the perturber, electron binding energy, density of nearby Rydberg states, and the radial extent of the orbital. Experimental probes and theoretical models of such interactions have been the subject of considerable research activity.[2] Most of this body of work has concentrated on understanding the scalar quantities of various collisional processes.

Scalar experimental and theoretical studies of Rydberg atom rare-gas collisions are available in the literature. Typically, collisional depopulation cross sections for an initial Rydberg level with a rare gas have been measured in cell experiments. Many of these experiments investigated the collisional removal of $ns$, $np$, and $nd$ states in an $l$-mixing process, thought to occur by an impulsive Rydberg electron-perturber interaction (i.e., low energy electron scattering). No final states were resolved. The rates of $l$-mixing collisions of Na $nd$ states scale as the geometric size of the Rydberg level at low $n$, but decrease as $n$ becomes larger.[3] However, Na $ns$ state collisional depopulation studies showed that the $Na^+$/rare-gas interaction was responsible for the $n$ changing collision since no dependence on the $n$ level (geometric cross section of the Rydberg state) was found.[4] A study of Rb $np$ collisional quenching by rare gases concluded that the cross sections were not explained solely by electron/rare-gas or ionic core/rare-gas interactions.[5] Concurrent with these experiments, theoretical probes of these systems were developed that have relied mainly on a low energy electron scattering model which is formulated by the impulse approximation plus free electron model. Here, it is assumed that the ionic core-perturber and electron-perturber interaction are short range with respect to the mean distance between the ionic core and the Rydberg electron. This assumption allows the ionic core-perturber interaction to be ignored and the Rydberg electron to be considered free. Qualitative agreement between several theoretical studies and the experimental $n$-dependent $l$-mixing cross sections was obtained.[6] Both theory and experiment showed that the cross section for He increased as the geometric size of the Rydberg orbital (scales as $n^4$) from $n=5$ to 10. For $n\geqslant10$, the cross section leveled off or decreased slightly. This trend in the magnitude of the $l$-mixing cross section with $n$ leads to the conclusion that the interplay among the ionic core, Rydberg electron, and perturber changes.[7] At lower $n$, the three participants act together as a whole and the $l$-mixing cross section scales as the Rydberg geometric cross section. At higher $n$, it is the electron-perturber interaction which dominates. Therefore, the cross section scaling is less than the geometric cross section. Alternatively, these observations were explained by

[a]NSF Postdoctoral Fellow, Chemistry 1992–94.
[b]Permanent address: Department of Physics, University of Iowa, Iowa City, Iowa 52242.
[c]Staff Member, Quantum Physics Division, NIST.

 0021-9606/95/102(24)/9532/5/$6.00 

Gallagher *et al.*[3] and others[8] in a classical free electron model. In this model, an increase in orbital period (scales as $n^3$) and a decrease in Rydberg electron velocity (scales as $n^{-1}$) will decrease the probability of the electron-perturber impulsive collision. Therefore, as $n$ increases, the perturber has a greater chance of moving through the Rydberg orbital without encountering the Rydberg electron, thus leading to a decrease in the $l$-mixing cross section.

In the studies reported here, much more information about the angular momentum mixing mechanism can be gleaned from the anisotropic behavior of the dynamical event. To understand the anisotropic properties of a collision, a vector correlation experiment is needed, where the atom is initially excited and aligned (oriented) with respect to the collision axis. If the Rydberg atom is prepared in an aligned (oriented) state, then the spatial extent as well as the angular shape of the electron charge cloud can determine the scattering properties.

We present results for the $(n,l)$ state-changing collision of a Rydberg calcium atom with Xe in a two-vector correlation experiment $[\mathrm{Ca}(4s17d\ ^1D_2)\rightarrow\mathrm{Ca}(4s18p\ ^1P_1)]$. The Na cell experiments cited above measured absolute cross sections for collisional depopulation as a function of $n$. Here, relative cross sections for population transfer from individual angular momentum levels of the initial state to a final state are measured. We employ stimulated emission detection to probe the final state population, which is referred to as the dump method. Other than selective field ionization[9] (SFI) and the resonant collision of Rydberg $K$ atoms,[10] we are not aware of any state-to-state dynamical experiments of Rydberg atom collisions. In the preceding paper,[11] use of the dump method is assessed. It is found that if the dump step is chosen such that all final state magnetic sublevels are equally dumped to an intermediate state, then a reliable two-vector correlation experiment is achieved. Interpretation of the results for the state-changing collision are discussed in terms of two theoretical models.

## II. EXPERIMENT

### A. Overview

The collision induced near-resonant state-to-state energy transfer process

$$\mathrm{Ca}(4s17d\ ^1D_2)+\mathrm{Xe}\rightarrow\mathrm{Ca}(4s18p\ ^1P_1)+\mathrm{Xe}+\Delta E = -1.7\ \ \mathrm{cm}^{-1} \quad (1)$$

is investigated in a crossed beam experiment which is schematically shown in Fig. 3 of Ref. 11. In the crossed beam apparatus the Ca atoms emanating from an effusive oven are electronically excited by a two-step laser excitation scheme, displayed in Fig. 1. At the interaction region the Ca beam is crossed at 90° with a pulsed supersonic jet of Xe atoms. This configuration provides a well defined initial relative velocity vector, $v_{\mathrm{rel}}$. The relative velocity of the Ca+Xe collision is 82 meV (718 m/s). The reader is referred to previous publications[12,13] for the details of the calcium effusive oven and pulsed jet. Upon collision, population that transfers to the collisionally produced $4s18p\ ^1P_1$ level is stimulated down to the $4s4d\ ^1D_2$ level with a third pulsed dye laser.

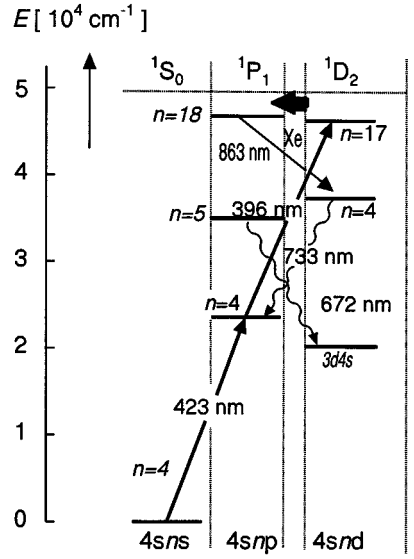


FIG. 1. Schematic representation of the energy levels for a Rydberg collision, where the final state is probed by the stimulated emission (termed the *dump* method in this paper). The subsequent fluorescence is measured as the initially aligned Rydberg orbital is rotated with respect to $v_{\mathrm{rel}}$.

Subsequent fluorescence from the $4s4d$ state to the $4s4p\ ^1P_1$ state at 733 nm is collected by a fiber optic bundle coupled to a monochromator and photomultiplier tube (PMT). No signal was observed with He as the collision partner, whereas the interaction with Xe provides adequate signal to extract an alignment effect.

### B. Ca($4s17d\ ^1D_2$) preparation

The $4s17d$ level is excited in a resonant two step excitation involving only singlet states $(4s^2\rightarrow4s4p\rightarrow4s17d)$. The angular wave function of the aligned state depends on the relative angles of the individual laser polarizations. With both laser polarizations parallel ($\updownarrow\updownarrow$), the Ca($^1D_2$) state is prepared with an angular wave function $Y_{20}$, where the laser polarization vectors serve as the quantization axis. When one laser polarization is set perpendicular to the other ($\updownarrow\leftrightarrow$), an aligned state with wave function $(Y_{2-1}-Y_{21})/\sqrt{2}$ is prepared. The probability density for the $n,l=17d$ Hydrogenic wave function $(|\Psi|^2=|R_{nl}Y_{lm}|^2)$ is shown in Fig. 2.

Two collinear pulsed dye laser beams are used to excite the initial state. Both dye lasers are pumped by a single Nd:YAG laser so that both photons reach the scattering center simultaneously, which improves the stability in the initial state population. The light emerging from the two dye lasers are linearly polarized vertically with respect to the laboratory frame. The polarization is refined by propagation through a Glan–Taylor prism. To prepare the $(Y_{2-1}-Y_{21})/\sqrt{2}$ angular wave function, one laser is directed through a double Fresnel rhomb to rotate the linear polarization by 90°. The two laser beams (423 and 396 nm) are combined by a beam splitter before the rotation by a second double Fresnel rhomb rotator. This can introduce some degree of ellipticity to the polarization because of differing amounts of retardation.

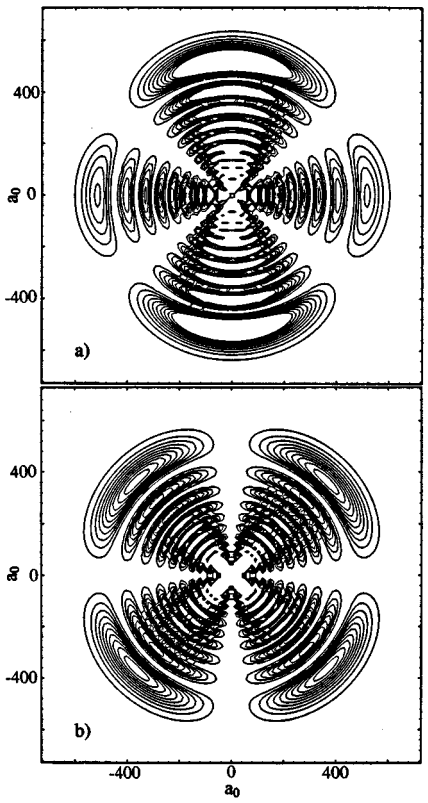


FIG. 2. Two-dimensional plot in bohr of the probability density $|\Psi|^2=|R_{nl}Y_{lm}|^2$ for the $17d$ level of hydrogen. (a) $Y_{20}$ spherical harmonic prepared by two parallel polarized lasers. (b) $(Y_{2-1}-Y_{21})/\sqrt{2}$ spherical harmonic prepared by two perpendicular polarized lasers.

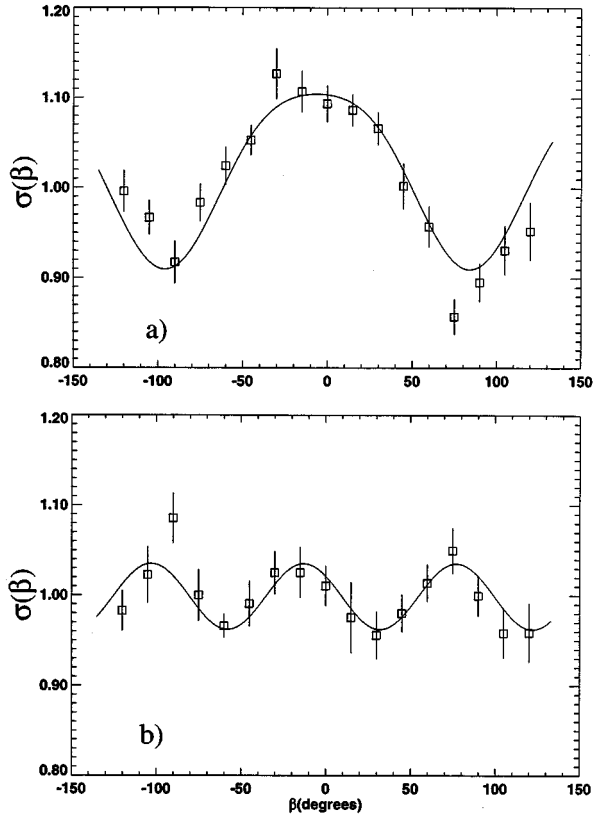


FIG. 3. Alignment data for the process $Ca(4s17d\ ^1D_2)+Xe \rightarrow Ca(4s18p\ ^1P_1)+Xe+\Delta E=-1.7\ cm^{-1}$ by dumping the final $Ca(4s18p\ ^1P_1)$ state. The two preparation lasers are aligned (a) parallel and (b) perpendicular. Error bars represent $1\sigma$ error.

### C. Stimulated emission detection

The final $4s18p\ ^1P_1$ state is probed by simulated emission. This method of detecting the collisionally produced final state is described in detail in the preceding paper.[11] To stimulate emission from the final $(4s18p\ ^1P_1)$ state to the $(4s4d\ ^1D_2)$ state, a wavelength of 863 nm is produced by a second Nd:YAG laser pumping a third pulsed dye laser. The dump laser pulse is passed through a Glan–Taylor prism to refine the linear polarization, which is vertical in the laboratory or space-fixed frame, because a small percent of the dye light is unpolarized amplified spontaneous emission. In this study, an elliptically polarized dump pulse is not required, as described in the preceding paper. The linearly polarized dump pulse is sufficient because it will stimulate emission from all three of the final $^1P_1$ state magnetic sublevels to the intermediate $^1D_2$ state. Fluorescence from the $^1D_2$ lower state at 733 nm is counted as a function of the angle that the prepared angular wavefunction makes with $v_{\rm rel}$, while the dump laser polarization is fixed with respect to the fiber bundle collection optics.

### D. Signal processing

The 733 nm photons are counted to obtain the population of the collisionally produced $4s18p$ state. Current from the PMT is amplified by 100 times and converted to a NIM voltage. The NIM voltage is converted to a frequency by a homebuilt pulse train stretcher in order to match the maximum input frequency of the computer expansion board counter. The pulse train stretcher counts the NIM pulses which arrive within an externally supplied time gate and outputs the counts as TTL with a 5 MHz frequency. This time gate is supplied by a pulse generator, triggered by the excitation laser pulse signal on a photodiode. The photon counting gate is delayed 20 ns from the dump laser pulse and is 50 ns wide, to maximize the ratio of collisionally produced photon counts to stray background counts. No direct fluorescence could be observed from the initially prepared $4s17d\ ^1D_2$ state. Therefore, to monitor the initial $^1D_2$ state, the cascade fluorescence light collected by the second fiber optic bundle is selected at 672 nm with a band pass filter and a second PMT. This PMT signal is gated 50 ns after the preparation laser pulse with a 100 ns width. The PMT current is integrated by a boxcar and converted to counts by a voltage-to-frequency converter. The final $4s18p$ data (after subtraction of background counts) are normalized to the $4s17d$ initial state fluorescence, giving alignment data that are proportional to the cross section $\sigma(\beta)$.

## III. RESULTS AND DISCUSSION

The cascade fluorescence from the dumped final state is collected as a function of the angle $\beta_{\rm rel}$ that the initial state makes with the initial relative velocity vector, $v_{\rm rel}$. Figure 3

TABLE I. Relative cross sections: $Ca(4s17d)+Xe \rightarrow Ca(4s18p)+Xe$.

| Detection method | Initial state polarization | Relative $m$-sublevel cross sections[a] $\sigma^0$ | $\sigma^{\|1\|}$ | $\sigma^{\|2\|}$ |
|---|---|---|---|---|
| Stimulated emission | Parallel ($\updownarrow$) | $1.13\pm0.02$ | $1.11\pm0.02$ | $0.83\pm0.02$ |
| Stimulated emission | Perpendicular ($\updownarrow\leftrightarrow$) | | $1.10\pm0.02$ | |

[a]Values normalized to $2J+1=5$ for $J=2$.

displays the alignment curves for laser polarizations parallel and perpendicular, respectively. Data were collected every 15° to resolve the fourfold structure. Approximately 30 alignment curves were averaged for the parallel and perpendicular configurations. The error bars represent the $\pm1$ standard deviation of the mean in the points. As described in the preceding paper,[11] in order to extract dynamical information about the energy transfer process, the following expression is used that relates the observed alignment curve to the fundamental $m$-sublevel cross sections ($\sigma^{|m|}$):

$$\sigma(\beta_{\mathrm{rel}})=\sum_m \left|\sum_{m'} g_{m'} d^{j=2}_{mm'}(\beta_{\mathrm{rel}})\right|^2 \sigma^{|m|}, \tag{2}$$

where $m$ and $m'$ are the magnetic quantum numbers of the initial state with respect to the initial relative velocity vector and the preparation laser polarization, respectively. The solid curves in the alignment data represent a nonlinear least-squares fit to Eq. (2). The relative values for the $m$-sublevel cross sections $\sigma^{|m|}$ are extracted from the alignment curves and are listed in Table I. The alignment data from the perpendicular wave function yields no new information and only uniquely determines the $\sigma^{|1|}$ value, as noted previously.[12]

The dynamical information of the collision is contained in the relative $\sigma^{|m|}$ cross sections. From Table I, we see that the $\sigma^{|0|}$ and $\sigma^{|1|}$ values are essentially equal in magnitude but significantly larger than the $\sigma^{|2|}$ value. In other words, the interaction between the $d_{z^2}$ electron charge cloud and the Xe atom is more likely to produce the $4s18p$ final state in an end-on collision than in a side-on collision. Interpretation of these results may be approached in several ways, and two viewpoints are considered here. The first interpretation is based on molecular Born–Oppenheimer potential curves of the transient van der Waals diatomic formed during the collision. The Born–Oppenheimer approximation may be valid at $n=17$ for the following reason. The root mean square velocity of the $n=17$ Rydberg electron is about $10^7$ cm/s, which is two orders of magnitude larger than the relative nuclear velocity of the Ca and Xe atoms, approximately $10^5$ cm/s. It is clear from the data that the initial asymptotic $\Sigma$ and $\Pi$ states corresponding to $\sigma^0$ and $\sigma^{|1|}$ are preferred for this state-changing collision. A recent semiclassical theoretical study[14] showed that the dependence of the initial orbital alignment of the state-changing collision of a Rydberg $Na(np)$ atom with He can be large and quite sensitive to the collision velocity (Stueckelberg oscillations). Unfortunately, van der Waals potentials for the $4s17d$ levels with Xe are not yet available. Lacking this information, the data can be analyzed only by an intuitive picture of the curve crossings. Because of the large density of states in the Rydberg series, however, it is very difficult to do so. It also becomes quite difficult to interpret because the van der Waals interaction potential is much greater than the 1.7 $cm^{-1}$ splitting between the initial and final states. Nevertheless, it is clear from the enhanced values of $\sigma^0$ and $\sigma^{|1|}$ that the asymptotic $\Sigma$ and $\Pi$ states are preferred in the entrance channel.

The second analysis invokes the impulse approximation in two frameworks: the free electron model[7,15] and a time-dependent perturbative approach.[16] In both frameworks, it is assumed that the electron and the perturber interact impulsively at short range because the large Rydberg electron charge cloud is unperturbed by the localized rare gas projectile until the moment of impact. Work is in progress to use the free electron model to predict observable alignment effects in the Rydberg collisions of Ca*+He.[15] Here the Rydberg electron and the cation core are considered as separate scatterers. The Rydberg electron/rare-gas perturber interaction is assumed to be the most important, and the other interactions are ignored. The state-changing process occurs through electron scattering with the rare-gas atom. The scattering amplitude for the state change is given by

$$f_{nlm\leftarrow n'l'm'}=4\pi f_{\mathrm{electron}}(Q)\langle n'l'm'|e^{i\mathbf{Q}\cdot\mathbf{r}}|nlm\rangle, \tag{3}$$

where $f_{\mathrm{electron}}(Q)$ is the electron/rare-gas scattering amplitude and the $e^{iQ\cdot r}$ is the momentum displacement operator. Basically, the magnitude of the overlap integral of the momentum displaced initial state and the final state governs the alignment effect.

Work is also in progress to use the time-dependent perturbation method to predict alignment effects[16] based on the impulsive collision between the Rydberg electron and the localized rare gas perturber. However, this approach takes a different tack than the free electron model (in momentum space). The semiclassical approach in configuration space is based on a time-dependent perturbation method where the potential, $\mathbf{V}(r)$, is a delta function at $r$, the point in space where the rare gas collides with the Rydberg electron. With this assumption, the important quantity is the product of the initial and final state wave functions at the point of impact. Preliminary results for $Ca(4s17d\ ^1D_2)+Xe$ (where the electron/Xe interaction is represented by the Fermi contact potential[17]) show that the individual $\sigma^{|m|}$ values vary significantly with velocity of the nuclei. The $\sigma^0$ value is large over some of that range and this result agrees well with our experimental results. Although it is unclear how these theories

will handle Xe given its larger size and polarizability, these preliminary theoretical results, in qualitative agreement with experimental data, are promising.

## ACKNOWLEDGMENTS

The authors are grateful to the National Science Foundation for support of this research. We also acknowledge support from the NATO collaboration Grant No. CRG 930833. The research of J.D. has been made possible by a fellowship of the Royal Netherlands Academy of Arts and Sciences. E.M.S. thanks Professor John Delos and Dr. Eric Layton for informative discussions on the theoretical aspects of this project. We are grateful to Harold V. Parks for generating the $17d$ hydrogenic orbital plots for this paper.

[1] E. Fermi, Nuovo Cimento **11**, 157 (1934).
[2] *Rydberg States of Atoms and Molecules*, edited by R. F. Stebbings and F. B. Dunning (Cambridge University Press, Cambridge, 1983), and references therein.
[3] T. F. Gallagher, S. A. Edelstein, and R. M. Hill, Phys. Rev. A **15**, 1945 (1977).
[4] T. F. Gallagher and W. E. Cooke, Phys. Rev. A **19**, 2161 (1979).
[5] F. Gounand, P. R. Fournier, and J. Berlande, Phys. Rev. A **15**, 2212 (1977).
[6] A. P. Hickman, R. E. Olson, and J. Pascale, in *Rydberg States of Atoms and Molecules*, Ref. 2, pp. 204–209.
[7] M. Matsuzawa, in *Rydberg States of Atoms and Molecules*, Ref. 2, p. 269.
[8] C. E. Burkhardt and J. J. Leventhal, Phys. Rev. A **43**, 110 (1991).
[9] See, for example, W. P. West, G. W. Foltz, F. B. Dunning, C. J. Latimer, and R. F. Stebbings, Phys. Rev. Lett. **36**, 354 (1976); F. G. Kellert, K. A. Smith, R. D. Rundel, F. B. Dunning, and R. F. Stebbings, J. Chem. Phys. **72**, 3179 (1980).
[10] M. J. Renn, W. R. Anderson, and T. F. Gallagher, Phys. Rev. A **49**, 908 (1994).
[11] E. M. Spain, M. J. Dalberth, P. D. Kleiber, S. R. Leone, S. S. Op de Beek, and J. P. J. Driessen, J. Chem. Phys. **102**, 9522 (1995).
[12] R. Robinson, L. J. Kovalenko, C. J. Smith, and S. R. Leone, J. Chem. Phys. **92**, 5260 (1990).
[13] J. P. J. Driessen, C. J. Smith, and S. R. Leone, J. Phys. Chem. **95**, 8163 (1991).
[14] B. C. Saha and N. F. Lane, Phys. Rev. Lett. **72**, 3487 (1994).
[15] W. Isaacs and M. A. Morrison (unpublished).
[16] E. Layton and M. A. Morrison, private communication (unpublished).
[17] J. I. Gersten, Phys. Rev. A **14**, 1354 (1976).